# Resonant tunneling in coupled quantum dots

C. Y. Fong
*Department of Physics, University of California, Davis, California 95616-8677*

J. S. Nelson
*Sandia National Laboratories, Albuquerque, New Mexico 87185*

L. A. Hemstreet
*Naval Research Laboratory, Washington, D.C. 20375-5000*

R. F. Gallup
*Department of Physics, University of California, Davis, California 95616-8677*

L. L. Chang and L. Esaki
*IBM Thomas J. Watson Research Center, Yorktown Heights, New York 10598*
(Received 24 April 1992)

We have applied a scaled version of the Kohn-Sham equations of density-functional theory to study the charge distribution at the condition of resonant tunneling in coupled quantum dots. We find that the tunneling process is governed by the symmetry properties of the resonantly coupled quantum-dot states. At resonance, the coupled atomiclike quantum-dot states form bonding and antibonding molecular resonant-tunneling states. The charge distribution of the bonding-type state is given. In addition, we find asymmetries of the charge in the barrier vs voltage (analogous to $I$-$V$ curves) as a result of electron-electron interactions between electrons in the excited tunneling and ground states.

## I. INTRODUCTION

Resonant tunneling (RT) in low-dimensional quantum nanostructures has recently attracted considerable attention due to the unique electronic and optical properties they exhibit.[1-10] With recent advances in microfabrication, it is now possible to make zero-dimensional quantum-dot (QD) nanostructures in which carriers are confined in all three dimensions. The electronic states of these structures resemble giant artificial atoms. RT in single-QD structures can occur through coupling of electronic states at the Fermi level of the emitter with the discrete levels of the QD.[2,3,11] As the emitter Fermi level is brought into resonance with the discrete QD states, an increase in current is observed. In double- or coupled-QD structures, RT can occur through several channels: (1) when the bias voltage brings discrete states of a single QD into resonance with the emitter Fermi level (a relatively weak channel due to non-RT through the other QD); (2) when the bias voltage brings two neighboring QD states into resonance; and (3) when the bias voltage brings resonantly coupled QD's into resonance with the emitter Fermi level. In the latter case, RT will occur across the entire structure. All three channels have been used to explain the fine structure observed in the tunneling current versus voltage ($I$-$V$) curves of samples composed of an emitter coupled to a column of QD's.[11]

Many of the theoretical models used to examine RT processes in quantum-well (QW) structures have been applied to QD RT.[11-16] In most cases, the $I$-$V$ curves are obtained by either calculating the transmission coefficients by matching the logarithmic derivatives of the wave function at the barrier, or by the density-matrix approach in which the current is expressed through the Fermi functions of neighboring wells. In the density-matrix approach, the applied voltage appears in the energy dependence of the Fermi functions and the detailed matching condition of the wave function does not explicitly appear. Neither approach clearly demonstrates how the electronic charge distribution varies as the bias voltage (the main driving force for the RT process) passes through resonance. Furthermore, although Presilla, Jona-Lasinio, and Capasso[16] have studied the effects of electron-electron interactions in double-barrier QW structures and several authors[17-19] have studied the electron-electron interactions in single QD's, the effect of the electron-electron interaction on the resonance voltage has not been considered for the case of coupled QD's.

In this paper, we use a self-consistent scheme based on a scaled version (dielectric and effective-mass scaling) of the Kohn-Sham equations of density-functional theory[20] to investigate RT in coupled or interacting QD nanostructures. The dynamics of the tunneling process are modeled by incrementally changing the static potential in each QD to simulate the effects of an applied voltage. In this way, the detailed nature of the wave-function evolution, illustrated through electron-charge-density contour profiles, can be investigated near resonance. In our scheme,[21] the electron-electron (Hartree and exchange-correlation) interaction is explicitly included through the local-density approximation (LDA) (Refs. 22 and 23) of density-functional theory.[20] In addition, by artificially

 

modifying the strength of the electron-electron interaction we are able to examine the effects of the electron-electron interaction on the strength of the bias voltage. Our studies also suggest the possibility of a light-switch device, based on control of the tunneling through modulation of the electron occupation in the QD array.

In the rest of the paper, a description of the computational supercell and scaled Kohn-Sham formalism is presented in Sec. II, in Sec. III we present and discuss our results, and in Sec. IV we summarize our work.

## II. COUPLED QD MODEL AND SCALED KOHN-SHAM METHOD

The computational supercell shown in Fig. 1 contains three GaAs rectangular QD's of dimension $a^2c$ separated by thin $Al_{0.5}Ga_{0.5}As$ barriers of length $d$, and surrounded by thick $Al_{0.5}Ga_{0.5}As$ barriers of width $b$. The 43-Å barriers $b$ are sufficiently thick to effectively isolate periodic arrays of dots in neighboring supercells, thereby allowing RT to occur only in the $z$ direction within a supercell. The lateral and longitudinal dimensions of a QD are arbitrarily taken as 81 and 133 Å, respectively. To allow sufficient tunneling to occur along the $z$ direction, the thin $Al_{0.5}Ga_{0.5}As$ barriers $d$ are taken as 8.4 Å. Thicker barriers drastically increase the computational time due to the weak wave-function overlap between the dots. Therefore, the total $x$, $y$, and $z$ dimensions of the supercell are 167, 167, and 502 Å respectively.

In our model system of coupled QD's given above, the potential in the $Al_{0.5}Ga_{0.5}As$ barriers are taken to be zero, while the inside GaAs rectangular QD's the potential is set at a constant value of $-37.7$ mRy, or about 50% of the GaAs/AlAs conduction-band discontinuity (900.0 meV).[21]

To simulate the tunneling process between the GaAs QD's under an applied voltage, we vary the static potential values in each QD linearly. To simplify the computation, we take an average of the linear potential within each QD and assume it to be constant within each QD. This simplification does not alter the general features of the RT process discussed below. For later reference, we label the three QD's, starting from left to right, as left-hand-side-dot (LHSD), the middle-dot (MIDD), and the right-hand-side-dot (RHSD), respectively.

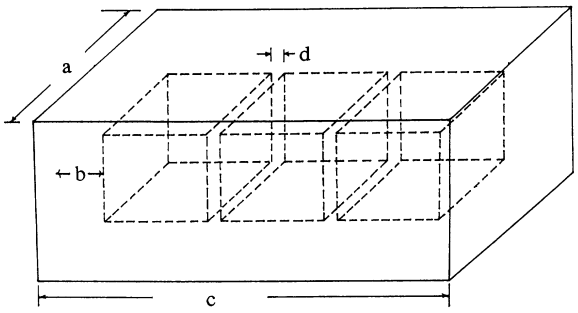


FIG. 1. Model of the computational supercell containing three quantum dots. The dimensions of the supercell are $a=167$ Å, $c=502$ Å, $b=43$ Å, and $d=8.4$ Å. The small value for the QD barrier $d$ allows for sufficient coupling between the QD states.

To calculate the electronic energies and charge densities, we employ a simple scheme[21] to scale the Kohn-Sham self-consistent equations of density-functional theory.[20] This scheme was developed by us to treat interacting electrons in quantum nanostructures with complicated boundary conditions. In Ref. 21, the QD is assumed to consist of a semiconducting dielectric such as GaAs, and interacting electrons within the QD derived from ionized donors. The electrons are assumed to be derived from a single isotropic, parabolic band ($k=0$, zone center) with an effective mass of $0.067m_0$ ($m_0$ is the free-electron mass), and to interact through a screened electron-electron interaction treated within the LDA of density-functional theory.[20] Let us first consider the Kohn-Sham one-electron equation:

$$\left[-\hbar^2/2m_0\nabla^2+V(\mathbf{r})+\int e^2\rho(\mathbf{r}')/|\mathbf{r}-\mathbf{r}'|d\mathbf{r}' + V_{\rm xc}[\rho(\mathbf{r})]\right]\Psi(\mathbf{r})=E_n\Psi(\mathbf{r}) . \quad (1)$$

The dielectric constant $\varepsilon$ and effective-mass scaling for the quantum-dot problem can be seen by replacing $m_0$ by $m^*$ and the interaction by the screened interaction, then applying a dimensional analysis. For example, using a value of 10 for $\varepsilon$, $m^*$ of $0.10m_0$, a potential $V(\mathbf{r})$ in units of (1/1000 Ry), and length units of 100 a.u., we can scale each term by (1/1000):

$$[(-\hbar^2/2)(1/0.1m_0)(1/100\text{ a.u.})^2\nabla^2]+(1/1000)V(\mathbf{r})+(e^2/\varepsilon)(1/100\text{ a.u.})^3 \times(1/100\text{ a.u.})(100\text{ a.u.})^3\int\rho(\mathbf{r}')/|\mathbf{r}-\mathbf{r}'|d\mathbf{r}'+(1/\varepsilon)(1/100\text{ a.u.})V_{\rm xc}[\rho(\mathbf{r})]\Psi(\mathbf{r})=E_n\Psi(\mathbf{r}) .$$

Then,

$$(1/1000)\left[(-\hbar^2/2m_0)\nabla^2+V(\mathbf{r})+e^2\int\rho(\mathbf{r}')/|\mathbf{r}-\mathbf{r}'|d\mathbf{r}'+V_{\rm xc}[\rho(\mathbf{r})]\right]\Psi(\mathbf{r})=E_n\Psi(\mathbf{r}) . \quad (2)$$

After the scaling, the energies $E_n$ are now in the units of mRy, and the length scales are in units of 100 a.u. A similar approach has been used by Ghazali and Hugon[24] to study the metal-insulator transition in doped semiconductors.

In this work, we have assumed that three electrons are contained in each supercell. Therefore, the lowest-energy state will be fully occupied and the second state will contain one electron. The second state, which is half occupied, will be referred to as the first excited state.

## III. RESULTS AND DISCUSSION

To illustrate the evolution of the wave-function near resonance, we present results for five applied voltages or potential differences between the LHSD, MIDD, and RHSD of $v_0$, $v_1$, $v_2$, $v_3$, and $v_4$; $v_0$ corresponds to zero applied voltage. Without the applied voltage, the potential in each QD is the same (−37.7 mRy), and for infinitely separated QD's the energy levels would be degenerate. Since we have made the barriers (d) relatively thin, 8.4 Å, the states in each QD can couple and the degeneracy is lifted. The $x$, $y$, and $z$ degeneracy is also removed by the rectangular symmetry of our QD's; the confinement energy in the lateral directions $(x,y)$ is larger than along the $z$ direction. As will be seen, a value of $v_2$ for the applied voltage corresponds to a near-resonance condition.

The electronic charge distribution of the lowest two eigenstates of the zero-field case $v_0$ are given in Fig. 2. The barriers are indicated by dashed lines so that the three QD's can be easily identified. The charge density of the lowest energy state $E_1$ [Fig. 2(a)] is symmetric with respect to the MIDD. The kinetic energy of the $E_1$ state is lowered by the spread of the symmetric charge distribution. The $E_1$ state can also be viewed as a linear combination of the lowest energy states of three uncoupled QD's. In Fig. 2(b), we depict the charge distribution of the first excited state (one-half occupied) $E_2$. This state can also be viewed as a linear combination of the lowest energy states of uncoupled QD's, but in this case, the charge density is localized in the LHSD and RHSD to reduce the Coulomb interaction with the $E_1$ state. The calculated splitting between $E_1$ and $E_2$ is 2.0 meV.

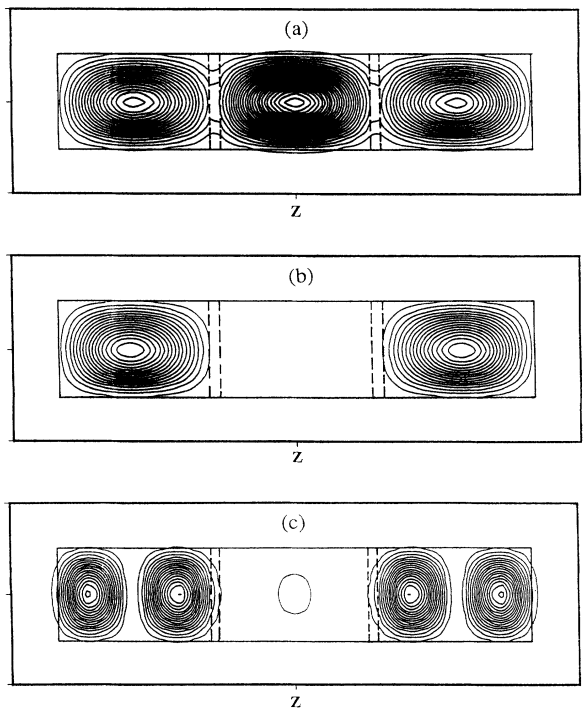


FIG. 2. Zero-field ($v_0$) charge-density contours in a (100) plane passing through the center of the computational supercell for (a) the fully occupied states, (b) the partially occupied first excited state, and (c) a higher-energy (fifth) excited state with $p_z$ symmetry.

The lowest occupied states $E_1$ and $E_2$ shown above represent linear combinations of isolated QD sinelike solutions. We also expect to see higher energy states that are linear combinations of isolated QD $p$-like solutions (single QD states with a node in the center of the QD). An example of a $p$-like state is given in Fig. 2(c). This state exhibits $p_z$ character in the LHSD and RHSD. Because of the rectangular symmetry of our QD's, similar states can be found at higher energy with $p_{x,y}$ character.

A schematic energy-level diagram summarizing the electronic energy levels in the zero applied voltage case is given in Fig. 3. The two groups of the threefold degenerate states are listed for finite $d$. In the presence of an applied voltage, these states become localized in a particular QD due to the Stark ladder effect[25] and the energy of the RHSD is lower than that of the MIDD, which in turn is lower than that of the LHSD. For convenience, we concentrate on the RT between the MIDD and the RHSD. With the assumption of three electrons in our system, energy level $E_1$ of the system, which is located in the RHSD, will be fully occupied by two electrons. The third electron will be in energy level $E_2$, which is localized in the MIDD. As the applied voltage is increased, level $E_2$ of the MIDD will move into resonance with $E_3$ whose charge density should exhibit $p_z$ character and is confined in the RHSD. Therefore, at resonance we should see a coupling of the $s$-like $E_2$ and the $p_z$-like $E_3$ states. Note, however, that in the following discussion, we will continue to refer to the state which is localized in the MIDD as $E_2$ and the state which is localized in the RHSD as $E_3$.

We now proceed to a more detailed discussion of the dot system under an applied dc electric potential of increasing strength. With a potential difference of $v_1 = 3.7$ mRy between the RHSD, MIDD, and LHSD, the two lowest eigenstates are $E_1$, which is localized in the RHSD, and $E_2$, which is localized in the MIDD. These states are shown in Figs. 4(a) and 4(b), respectively. The

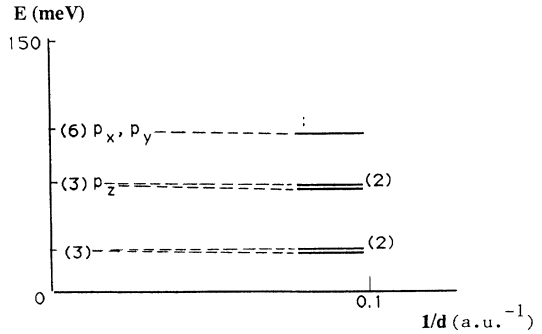


FIG. 3. Schematic energy-level diagram for the zero-field case ($v_0$). Numbers in brackets are the degeneracies. $p_x$, $p_y$, and $p_z$ are referred to the symmetry of the states in an isolated dot ($d \rightarrow \infty$).

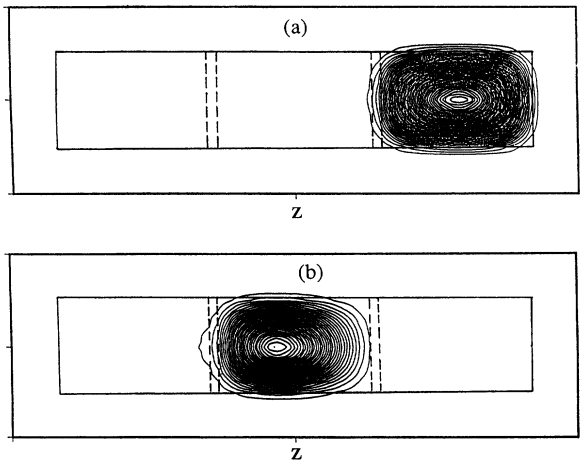


FIG. 4. Charge-density contours (same plane as Fig. 2) for an applied voltage of $v_1=3.7$ mRy. The two lowest states for this applied voltage are the sinelike "uncoupled" QD states $E_1$ of the RHSD (a) and $E_2$ of the MIDD (b).

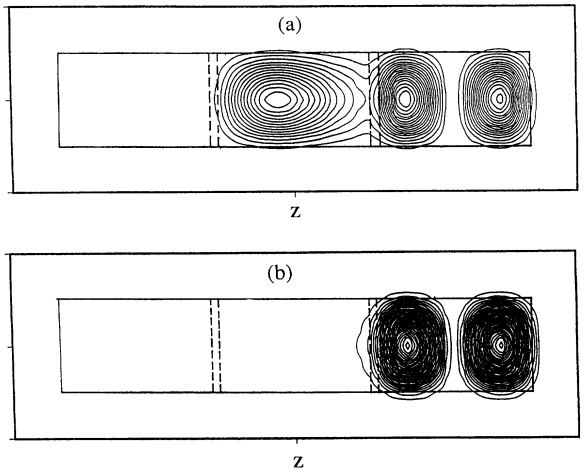


FIG. 6. Charge-density contours for applied voltages of $v_3=8.14$ mRy (a) and $v_4=11.5$ mRy (b). Voltage $v_3$ is just above resonance and $v_4$ well out of resonance.

coupling between the low-energy states, which is evident in the zero-field case (Fig. 2), has been removed, and the states are completely localized in one of the QD's. A potential difference of $v_1=3.7$ mRy is not large enough, however, to bring $E_2$ of the MIDD in resonance with the $E_3$ state of the RHSD.

By further increasing the potential difference to $v_2=7.4$ mRy, states $E_2$ and $E_3$ are brought into resonance. The discrete QD states $E_2$ and $E_3$ combine to form bondinglike and antibondinglike molecular RT states with a splitting of 4.0 meV. The charge density of the bonding state is depicted in Fig. 5, and clearly demonstrates the resonance condition. The density is evenly distributed over the MIDD and RHSD. Furthermore, the symmetric character of the $E_2$ state in the MIDD dot and the $p_z$ character of the $E_3$ state in the RHSD is maintained at resonance. In fact, tunneling can only occur between these states because of the wave-function matching condition at the barrier: specifically, neither wave function has a node in the $xy$ plane. In contrast, the lowest-energy $E_2$ state of the MIDD cannot couple to $p_x$- or $p_y$-like states in the RHSD, since their lobes point in the $xy$ directions and the additional nodes

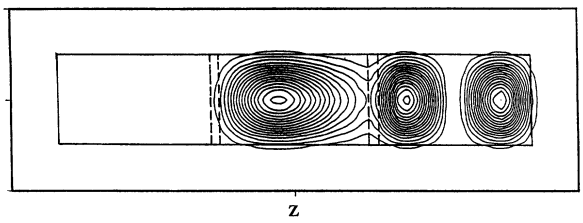


FIG. 5. Charge-density contours (same plane as Fig. 2) of the bonding resonance state, $v_2=7.4$ mRy (coupling of the $E_2$ state of the MIDD and the $E_3$ state of the RHSD). Note the even distribution of this state over the MIDD and RHSD, and the retention of the symmetry of the individual states at resonance.

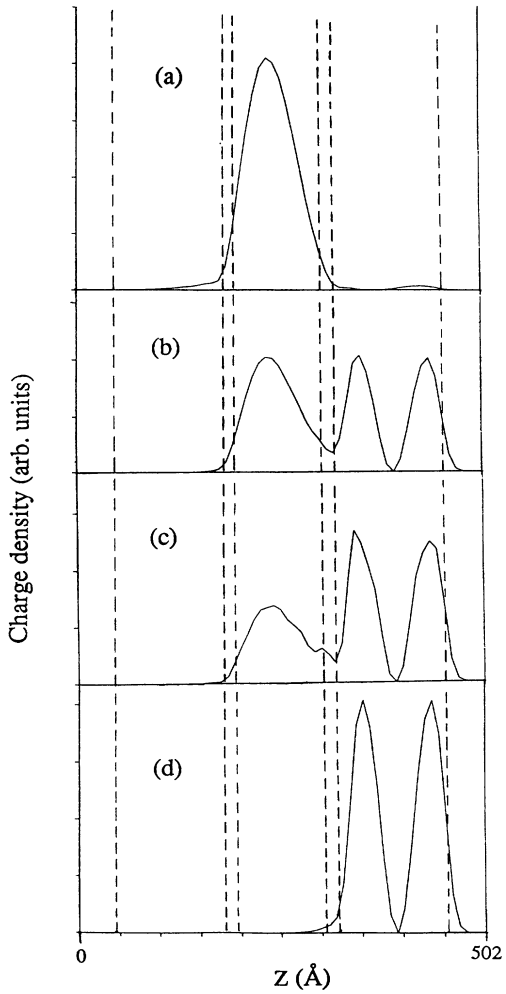


FIG. 7. Charge-density profiles along the [001] direction for applied voltages $v_1$–$v_4$. Notice the evolution of the charge density from the sinelike $E_2$ state in the MIDD to the $p_z$-like $E_3$ state in the RHSD. (a) $v_1=3.7$ mRy; (b) $v_2=7.4$ mRy; (c) $v_3=8.14$ mRy; and (d) $v_4=11.5$ mRy.

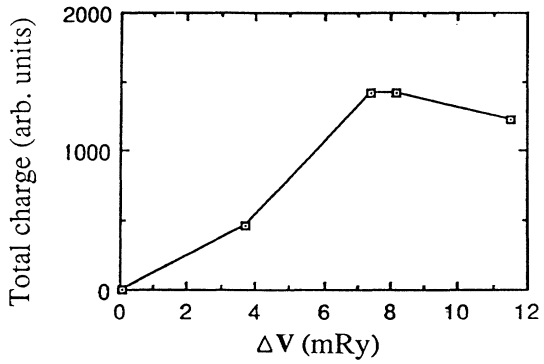


FIG. 8. Barrier charge between the MIDD and the RHSD vs applied voltage. We use this as a static measure of the current flow from the MIDD to the RHSD as the voltage is passed through resonance. The asymmetric shape of the curve is a result of the electron-electron interactions between the tunneling electrons ($E_2$ or $E_3$ states) and the completely occupied $E_1$ state of the RHSD.

in the $xy$ plane cannot match the $E_2$-state wave function in the MIDD.

With further increases in the potential difference to $v_3 = 8.14$ mRy (just above resonance) and $v_4 = 11.5$ mRy (well above resonance), the $E_2$ and $E_3$ states are brought out of resonance and are in reverse order. The charge distributions of the first excited state (either $E_2$ or $E_3$) for voltages of $v_3$ and $v_4$ are given in Figs. 6(a) and 6(b), respectively. For an applied voltage of $v_3$, the $E_3$ state of the RHSD is slightly lower in energy than the $E_2$ state of the MIDD. Although the states still exhibit a resonance character, the corresponding charge density is more localized in the RHSD. At an applied voltage of $v_4$, the states are completely uncoupled: the $E_3$ state is lower in energy than the $E_2$ state of the MIDD and is localized in the RHSD.

The dynamics (or sequence of static profiles) of the charge evolution between the MIDD and RHSD for voltages $v_1$–$v_4$ are summarized in Fig. 7. As discussed above, the distribution changes from the symmetric $E_2$ state in MIDD [Fig. 7(a)], to the resonance condition between $E_2$ and $E_3$ [Fig. 7(b)], and to the $p_z$ ($E_3$) state in the RHSD [Fig. 7(d)].

Since we have performed static calculations to simulate the quasisteady-state flow of charge in the RT process, we can use a static criterion as a measure of the RT condition. Our criterion is taken as the value of the total charge in the barrier between the MIDD and the RHSD; this quantity is plotted in Fig. 8. The maximum of the barrier charge occurs at the resonance potential value $v_2$, although the shape of the curve is not symmetric. This asymmetry is caused by electron-electron interactions between the first excited states, $E_2$ or $E_3$, and the lowest-energy state $E_1$, which is fully occupied and localized in the RHSD. As the potential difference passes through the resonance condition, electrons flowing to the RHSD from MIDD are repelled by the Coulomb interaction with the $E_1$ state in the RHSD. Furthermore, the electron-electron interaction affects the value of the resonance voltage. A smaller value of the resonance voltage is expected when electron-electron interactions are neglected. To test this expectation, we reduced the electron-electron interaction to 1% of its normal value and searched for the new resonance voltage. The new voltage was found to be one-half (3.7 mRy) the value obtained using the full electron-electron interaction (7.4 mRy).

The sensitivity of the RT voltage to the electron-electron interactions suggests the possibility of a light-switch device, which could be made by controlling the occupation of the electrons in the ground state (in our case this would be the $E_1$ level in the RHSD). If electrons can be removed from the ground state, the tunneling electrons, i.e., electrons flowing from the MIDD to the RHSD, can make a transition from the $p_z$ ($E_3$) state to the ground state $E_1$ with the emission of light. The dipole matrix element will be large, since the transition occurs between even and odd states within the RHSD. The radiation can be stopped by injecting electrons into the ground state of the RHSD.

## IV. SUMMARY

In summary, we have applied a scaled version of the Kohn-Sham equations of density-functional theory to study the evolution of charge distribution at RT in coupled QD's. We have shown that the tunneling process is governed by the symmetry properties of the resonant states. At resonance, the coupled atomiclike QD states form bonding and antibonding molecular RT states. In addition, we have found asymmetries of the charge in the barrier vs voltage (analogous to $I$-$V$ curves) as a result of electron-electron interactions between the tunneling electron and ground-state electrons. Finally, our results have demonstrated that it is possible to obtain qualitative dynamical information concerning transport properties from static calculation, when the processes involved are in a quasi-steady-state.

## ACKNOWLEDGMENTS

C.Y.F. would like to thank the Sandia National Laboratories for financial support. This work was partially supported (J.S.N.) by the U.S. Department of Energy under Contract No. DE-AC0476P00789, and the U.S. DOE Office of High Performance Computing and Communications. L.A.H. would like to thank Office of Naval Research for support.

[1]L. Easki and R. Tsu, IBM J. Res. Dev. **14**, 61 (1970).
[2]J. N. Randall, M. A. Reed, R. J. Matyi, and T. M. Moore, J. Vac. Sci. Technol. B **6**, 1861 (1988).
[3]S. Tarucha, Y. Hirayama, T. Saku, and T. Kimura, Phys. Rev. B **41**, 5459 (1990).
[4]H. Y. Sheng and J. Sinkkonen, Superlatt. Microstruct. **7**, 341 (1990).
[5]H. Xu, Y. Wong, F. Zhang, and G. Chen, Phys. Status Solidi

B **163**, K25 (1991).
[6]W. Hansen, T. P. Smith III, K. Y. Lee, J. A. Brum, C. M. Knoedler, J. M. Hong, and D. P. Kern, Phys. Rev. Lett. **62**, 2168 (1989).
[7]Ch. Sikorski and U. Merkt, Phys. Rev. Lett. **62**, 2164 (1989).
[8]U. Sivan and Y. Imry, Phys. Rev. Lett. **61**, 1001 (1988).
[9]K. Kern, D. Heitmann, P. Grambow, Y. H. Zhang, and K. Ploog, Phys. Rev. Lett. **66**, 1618 (1991).
[10]For example, see *Science and Engineering of One- and Zero-Dimensional Semiconductors,* Vol. 214 of *NATO Advanced Study Institute Series B: Physics,* edited by S. P. Beaumont and C. M. Sotomayer Torres (Plenum, New York, 1990).
[11]G. W. Bryant, Phys. Rev. B **44**, 3064 (1991).
[12]A. Lorke, U. Merkt, F. Malcher, W. Weimann, and W. Schlapp, Phys. Rev. B **42**, 1321 (1990).
[13]A. Kumar, S. E. Laux, and F. Stern, Phys. Rev. B **42**, 5166 (1990).
[14]B. Ricco and M. Y. Azbel, Phys. Rev. B **29**, 4356 (1984).
[15]H. Schneider, K. von Klitzing, and K. Ploog, Superlatt. Microstruct. **5**, 383 (1989).
[16]C. Presilla, G. Jona-Lasinio, and F. Capasso, Phys. Rev. B **43**, 5200 (1991).
[17]P. A. Maksym and T. Chakraborty, Phys. Rev. Lett. **65**, 108 (1990).
[18]U. Merkt, J. Huser, and M. Wagner, Phys. Rev. B **43**, 7320 (1991).
[19]D. Pfannkucke and R. R. Gerhardts, Phys. Rev. B **44**, 13 132 (1991).
[20]W. Kohn and L. J. Sham, Phys. Rev. **140**, A1133 (1965).
[21]C. Y. Fong, R. F. Gallup, J. S. Nelson, L. L. Chang, and L. Esaki, Superlatt. Microstruct. (to be published).
[22]D. M. Ceperley and B. J. Alder, Phys. Rev. Lett. **45**, 566 (1980).
[23]J. P. Perdew and A. Zunger, Phys. Rev. B **33**, 5048 (1981).
[24]A. Ghazali and P. Leroux Hugon, Phys. Rev. Lett. **41**, 1569 (1978).
[25]See, for example, C. Y. Fong, R. F. Gallup, L. Esaki, and L. L. Chang, Superlatt. Microstruct. **7**, 147 (1990).